

PCCP

Accepted Manuscript



This is an *Accepted Manuscript*, which has been through the Royal Society of Chemistry peer review process and has been accepted for publication.

Accepted Manuscripts are published online shortly after acceptance, before technical editing, formatting and proof reading. Using this free service, authors can make their results available to the community, in citable form, before we publish the edited article. We will replace this *Accepted Manuscript* with the edited and formatted *Advance Article* as soon as it is available.

You can find more information about *Accepted Manuscripts* in the [Information for Authors](#).

Please note that technical editing may introduce minor changes to the text and/or graphics, which may alter content. The journal's standard [Terms & Conditions](#) and the [Ethical guidelines](#) still apply. In no event shall the Royal Society of Chemistry be held responsible for any errors or omissions in this *Accepted Manuscript* or any consequences arising from the use of any information it contains.

Electronic surface states and dielectric self-energy profiles in colloidal nanoscale platelets of CdSe[†]

Jacky Even,^{*a} Laurent Pedesseau,^a Mikael Kepenekian^{*b}

Received Xth XXXXXXXXXXXX 20XX, Accepted Xth XXXXXXXXXXXX 20XX

First published on the web Xth XXXXXXXXXXXX 200X

DOI: 10.1039/b000000x

The electronic surface states and dielectric self-energy profiles in CdSe colloidal nanoscale platelets are explored by means of an original *ab initio* approach. In particular, we show how the different coatings deeply modify the quantum and dielectric confinement in CdSe nanoscale platelets. Molecular coating leads to an electronic band gap free of electronic surface states as well as an optimal surface coverage. The reduced blinking in CdSe nanoscale platelets is discussed. The theoretical method here proposed allows one to go beyond the popular empirical description of abrupt dielectric interfaces by explicitly describing the nanoplatelet surface morphology and polarisability at the atomic level. This theoretical study opens the way toward more precise description of the dielectric confinement effect in any hybrid system exhibiting 2D electronic properties.

Introduction

Since the seventies, researchers have been able to grow semiconductor devices that exploit the quantum-mechanical behavior of carriers.^{1,2} Thin-film semiconductor crystal-growth techniques such as molecular beam epitaxy (MBE) led to the design of ultra-thin semiconductor layers and 2D quantum confined quantum well (QW) structures. Highly complex optoelectronic structures for light emission, like quantum cascade lasers are now routinely available.³ Electrical and optical injection of carriers, emission wavelength tuning, semiconductor alloying for electrical and optical confinements, etching techniques as well as doping, are necessary for numerous applications ranging from light emission, light detection, photovoltaics, high-speed nonlinear optical telecommunications, to mid-infrared sensing.^{1–7} Free standing colloidal nanoplatelets (CNPL) have recently emerged as a novel class of semiconductor nanostructures with two-dimensional electronic structures. These new nano-objects have attracted increasing interest thanks to their ease of synthesis, opening new routes for low-cost technologies. Among the most attractive physical properties of CNPL is the high quantum yield for light emission at room temperature after optical excitation. CNPL are also the fastest colloidal fluorescent emitters, reaching nanosecond radiative lifetime at low temperature.⁸

Time resolved optical spectroscopy studies are dedicated to the understanding of the blinking phenomenon which is only suppressed at low temperature, as well as the influence of non-radiative Auger effects.^{9–13} Despite foremost recent experimental research efforts, the understanding of underlying CNPL properties remains scanty. The design of more efficient CNPL structures requires a realistic modeling including chemical composition, mechanical, electrical and optical features.

The description of CNPL mono-electronic states rely either on the envelope function approximation coupled to the $k \cdot p$ perturbation method,^{8,14,15} on empirical tight-binding (TB) modeling¹⁵ or density functional theory (DFT) computation.¹⁶ The former approach yields a convenient way to quickly simulate the electronic properties, the electron-phonon interaction or the influence of the morphology, but fails to accurately describe properties down to the atomic scale. This is especially important for the ligands at the surfaces which play a major role in CNPL. The $k \cdot p$ method is also fundamentally not able to address properly the issue of non-parabolicity in the electronic dispersion which is important in ultrathin CNPL.¹⁵ TB gives a more accurate description of the electronic structure at the atomic level, but only up to now for the semiconductor core. It is nevertheless able to predict quantum confinement effect more precisely than the $k \cdot p$ method. DFT calculations are able to handle the whole CNPL structure, but this simulation technique suffers from the large underestimation of the electronic band gap in ground-state computation. This can be corrected by including many-body effects by means of self-energy correction $\Sigma = GW$ for the bulk electronic band gap,^{16,17} or by using the Bethe Salpeter equation resolution for the exciton contribution to the optical band gap.¹⁸ Unfortunately, such calcula-

[†] Electronic Supplementary Information (ESI) available: Complementary information on the 4-step procedure: variation of the induced dipole $m_z(L)$, smoothing of the Hartree potential. See DOI: 10.1039/b000000x/

^a Université Européenne de Bretagne, INSA, FOTON UMR 6082, 35708 Rennes, France; E-mail: jacky.even@insa-rennes.fr

^b Institut des Sciences Chimiques de Rennes, UMR 6226, CNRS - Université de Rennes 1, Campus de Beaulieu, 35042 Rennes, France; E-mail: mikael.kepenekian@univ-rennes1.fr

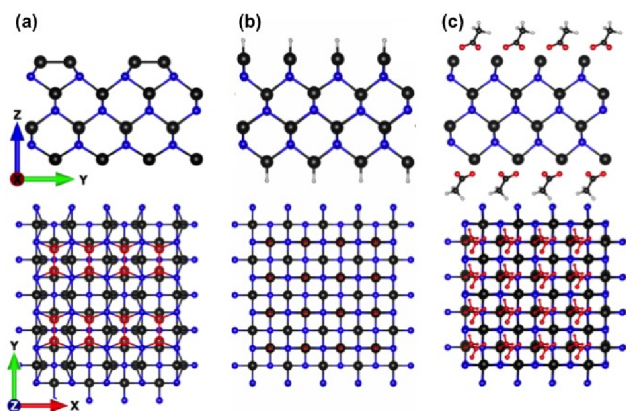


Fig. 1 Top and side view of CdSe CNPLs considered in this work. Cd, Se, O, C and H atoms are depicted in black, blue, red, gray and white, respectively. In the bottom pictures, top atoms (or molecules) are depicted in red. The (001) Cd surfaces at both ends are terminated by (a) a (2×1) surface reconstruction, (b) a H-passivated surface, and (c) a AcO-passivated surface.

tions are beyond available computational resources for large hybrid systems like CNPL.¹⁹

The unique optoelectronic properties of CNPL are especially related to the large dielectric contrast between the semiconductor and its ligand environment. This interaction strongly renormalizes bare single particle states and increases the electronic band gap. It can only be included into electronic modeling,^{14,15} by adding an empirical surface correction $\delta\Sigma$ to the self-energy of the carriers in the bulk material, which is related to the polarisability of the electron gas at the surface of the CNPL. The same effect strongly enhances the electron-hole interaction, leading to larger exciton binding energies up to several hundred meV and a reduction of the optical band gap. Despite the importance of these effects, nowadays empirical modeling of self-energy corrections rely on a simple representation of abrupt dielectric interfaces, with one dielectric constant value for the semiconductor core and another one for the surfaces and the surrounding medium.^{14,15} Alternatively, DFT-based theoretical methods were first proposed to calculate atomic-scale dielectric permittivity profiles across interfaces in free-standing silicon/oxyde and ferroelectric slabs.^{20,21} These calculations were later extended to include more complex heterostructures.²² Most of the DFT approaches are based on periodic supercells and plane wave representations of the electronic wavefunction. In that case, the size of the supercell is severely limited by the available computational resources. A saw-tooth representation of the external electric potential is necessary to minimize dipole-dipole interactions between the neighbouring slabs.²⁰ This numerical procedure is included in the self-consistent part of widely used first-principles codes such as VASP²³ and QUANTUM-

ESPRESSO.²⁴ A much less known computational method has been proposed to compute the dielectric permittivity of nanostructures by using first principles density functional perturbation theory in the SIESTA code.^{25–27}

The purpose of the present work is to propose an advanced description of the quantum confinement, the electronic surface states and the dielectric confinement starting from an atomistic modeling of the CNPL at the DFT level. The electronic wavefunctions are represented on a local basis, well-suited for inorganic-organic hybrid materials like CNPL. The influence of the electronic surface states on the CNPL electronic band structure is studied. The polarization induced by an external field for an isolated CNPL is then calculated after a correction of the electrostatic interactions between CNPL. A nanoscopic averaging procedure is used to obtain a dielectric constant profile along the stacking axis beyond the classical abrupt interface model. Self-energy profiles are deduced from a numerical procedure involving a transfer matrix approach. With this complete approach, we will show that it is possible to study the dielectric properties of a whole CNPL and incorporate various effects at the atomic level, including the influence of the CNPL thickness or the structure of the interface with the inspection of three different surface dressing (Fig. 1). Eventually, we show that acetate coating of CdSe CNPL leads not only to an optimal coverage, but also to enhance electronic properties.

Computational details

First-principles calculations are based on DFT as implemented in the SIESTA package.^{26,27} Calculations have been carried out with the GGA functional in the PBE form,²⁸ Troullier-Martins pseudopotentials,²⁹ and a basis set of finite-range numerical pseudoatomic orbitals for the valence wave functions.³⁰ Structures relaxation and electronic structure calculations have been done using a double- ζ polarized basis sets.³⁰ The geometries were optimized until the forces were smaller than $0.01 \text{ eV.}\text{\AA}^{-1}$. The electronic structure was converged using a $1 \times 5 \times 5$ k -point sampling of the Brillouin zone. In all cases, an energy cutoff of 150 Ry for real-space mesh size has been used.

Results & Discussion

CNPL band structure and electronic surface states

Starting from CdSe slabs such as both ends are terminated by a (001) surface of Cd atoms, we consider 3 different surfaces (Fig. 1): (a) a bare surface with a 2×1 reconstruction based on Cd dimers, (b) an hydrogen passivated surface where every Cd dangling-bonds is saturated, and (c) an acetate (AcO) passivated surface. Each structure has been built with different

thickness depending on the number, of repeated CdSe zinc-blende unit cells (each unit cell contains two CdSe monolayers (ML)).

The 2×1 (001) surface reconstructions are commonly observed in MBE grown samples of semiconductors.^{31,32} In this case, it consists in a succession of rows of Cd dimers (Fig. 1-a). The enlargement of the cell from 2×1 to 2×2 does not lead to a more stable buckled structure. The H-passivated structure corresponds to the complete passivation of Cd dangling-bonds (Fig. 1-b). The AcO-passivated structure considered here corresponds to the maximum coverage possible. It has already been under study in the case of CdSe colloidal nanocrystals (CNC).³³ In the case of nanoplatelets we find a similar arrangement with molecules in a tilted bridge configuration between two neighbouring Cd atoms (Fig. 1-c). This arrangement was found to stabilize the (001) facets in CdSe CNC.³³ Complete surface coverage and saturation of dangling-bonds are possible in the case of AcO-passivated CdSe CNPL, contrary to CdSe CNC (Fig. 1-c). The elimination of dangling-bonds prevents from the occurrence of surface states in the middle of the gap. As previously studied by Voznyy and coworkers, those strongly localized states act as traps, *i.e.* all of those states have to be emptied before excitonic emission becomes possible. Therefore, the saturation of dangling-bonds might be a first explanation for the reduced blinking phenomenon.^{33,34}

Fig. 2 presents the band structures for different coating of CdSe slabs. In the case of the thinnest CNPL ($n_{cell} = 1$), we find that the reconstructed (2×1) surface displays an indirect band gap ($\Delta E = 1.00$ eV), whereas both H-passivated and AcO-passivated surfaces show direct band gaps (1.31 and 0.98 eV, respectively). Both the indirect band gap for the reconstructed surface and, the large direct band gap for the H-passivated surface, are related to electronic surface states contributions close to the electronic band gap (Fig. 3). On the contrary, electronic states at the conduction and valence band edges are located inside for ultrathin CNPL with AcO-passivated surfaces. It shows that AcO-passivation as a beneficial effect on the optical properties of CNPL. The electronic band gap remains free of electronic surface states, thus reducing the possibility of non-radiative electronic recombination as well as avoiding Fermi level pinning at the surface. The blinking which is usually interpreted as a transfer of photogenerated electron and hole between CNC core states and surface states, is then expected to be reduced for CNPL.¹¹

It is well-known that DFT band gaps can be off by as much as a factor of 2 in semiconductors. Nevertheless, the qualitative trends are usually well reproduced. When going to thicker nanoplatelets ($n_{cell} = 3$) we can monitor the expected reduction of the band gaps (0.67 and 0.53 eV for the reconstructed and AcO-passivated surfaces, respectively). Moreover in the case of the (2×1) reconstruction we observe a displacement

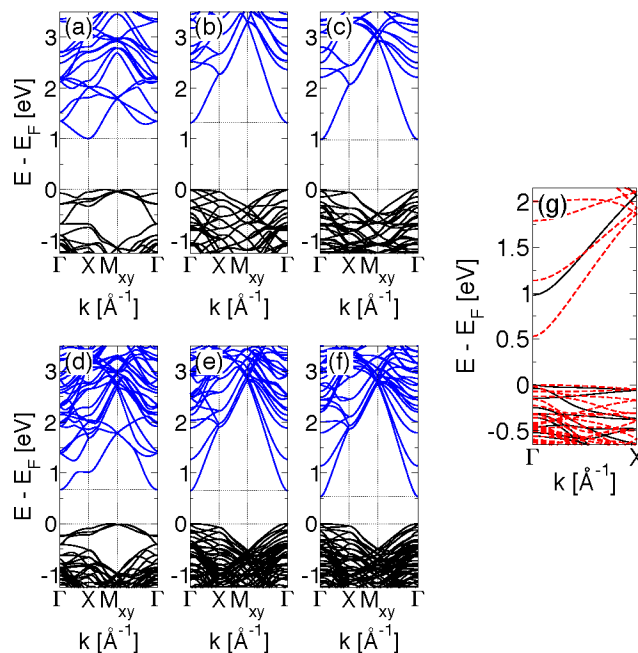


Fig. 2 Band structures of $n_{cell} = 1$ CNPL with (a) the reconstructed surface, (b) the H-passivated surface, (c) the AcO-passivated surface, and band structures of $n_{cell} = 3$ CNPL with (d) the reconstructed surface, (e) the H-passivated surface, (f) the AcO-passivated surface. Black and blue lines stand for occupied and empty bands, respectively. Dotted lines are guides to the eyes. (g) Band structures of the AcO-passivated surface for $n_{cell} = 1$ (plain black lines) and $n_{cell} = 3$ (red dashed lines). $n_{cell} = 3$ bands are shifted to help the comparison. In the case of the reconstructed surface, the thicker cell displays a reduced band gap as well as a displacement of the conduction band minimum from X to Γ .

of the conduction band minimum from X to Γ (Fig. 2-d). Indeed, the small effective masses of bulk CdSe at the Γ point lead to a much larger quantum confinement effect than at the X point. However, for ultrathin CNPL, quantum confinement effects can not be completely predicted on the basis of the electronic properties of bulk CdSe crystal. AcO-passivated CNPL exhibit a reduction of the influence of electronic surface states on the quantum confinement. Fig. 2-g presents a comparison of $n_{cell} = 1$ and $n_{cell} = 3$ AcO-passivated CNPL close to Γ . One can observe the reduce effect of the thickness on the valence bands, whereas the change of curvature of conduction bands is important. The feature of dielectric confinement will in turn be scrutinized in the next section.

Dielectric and self-energy profiles in heterostructures: a mixed approach

The atomic description of CNPLs presented in this work allows us to go beyond the crude continuum modelling of di-

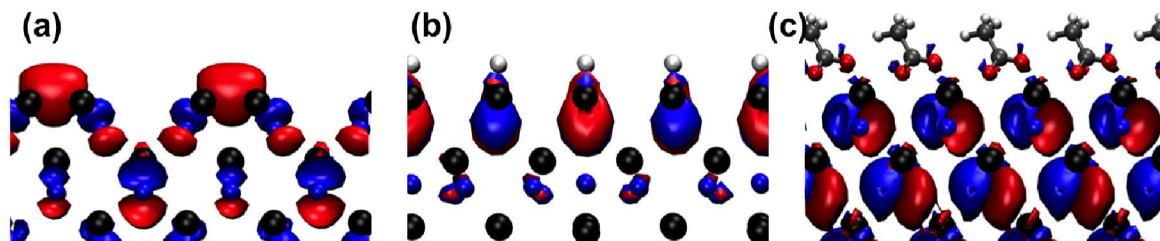


Fig. 3 Plot of the wavefunction at the valence band maximum for the upper half of CNPL ($n_{cell} = 1$) with (a) the reconstructed surface, (b) the H-passivated surface, and (c) the AcO-passivated surface. Red and blue lobes correspond to the positive and negative phases of the real part. The imaginary part is null for (b) and (c) (taken at the Γ point). In (a) the imaginary part is exactly superposed with the real one, and therefore cannot be seen on this plot. The wavefunction is localized at the surface for the reconstructed and H-passivated surfaces, whereas it is located inside the CNPL with the AcO-passivated surface.

electric heterostructures by abrupt interfaces.^{15,35,36} The first step consists in a DFT modelling of the electronic density induced by an external electric field. Dielectric continuum theory and nanoscale averaging are then used in a second step to extract dielectric and self-energy profiles along the stacking axis of the heterostructure. A complete quantum description of these properties is in principle possible using DFT theory and many-body effects.³⁷ Unfortunately, such calculations for heterostructures are beyond standard computational resources.³⁸ Moreover, appropriate approximations of *ab initio* theory for the dielectric and self-energies are still under debate for model periodic systems.³⁹

In many-body perturbation theory of bulk materials, single-particle removal/addition energies ϵ^{QP} , known as quasiparticle (QP) energies, have to be obtained either by perturbation or from an equation, containing a non-local self-energy operator $\Sigma(\vec{r}, \vec{r}', \epsilon^{QP})$ in which the exchange-correlation effects are contained.^{37,40} Non-local effects ($\vec{r} \neq \vec{r}'$) appear in the standard *GW* approximation of the self-energy operator,

$$\Sigma(\vec{r}, \vec{r}', \epsilon^{QP}) = i \int \frac{dE'}{2\pi} e^{-i\delta E'} G(\vec{r}, \vec{r}', E - E') W(\vec{r}, \vec{r}', E')$$

through the one-electron Green function G and the screening of the Coulomb interaction W due the non-locality of the microscopic dielectric constant.⁴¹ The degree of non-locality in the self-energy operator is measured primarily by its range, which is on the order of a bond length in semiconductors and insulators.⁴² The static Coulomb-hole screened exchange (COHSEX) approximation for the *GW* self-energy is a useful reference point for understanding the interplay of local fields and non-locality in such materials.⁴¹ The local fields arise from the microscopic response of the inhomogeneous charge density in the crystal to a perturbation. They are described by the off-diagonal elements of the microscopic dielectric matrix. Indeed, the nonlocal dielectric constant $\epsilon(\vec{r}, \vec{r}')$ yields a Fourier transform $\epsilon_{G,G'}(q)$ for a periodic solid (G, G' are reciprocal wavevectors, q is confined in the first Brillouin zone).

The full microscopic matrix $\epsilon_{G,G'}(q)$ thus contains informations related to local field effects mainly associated to tightly bound electrons.⁴³⁻⁴⁵ Local field effects are automatically included in the computation of the induced charge density for the methods based on the perturbation by an external field, such as the one proposed in this paper.⁴⁶

The connection between the microscopic dielectric constant $\epsilon_{G,G'}(q)$ for a bulk periodic solid and a Fourier component $\epsilon_M(q)$ with a short wavevector q of the macroscopic dielectric constant for an homogeneous medium $\epsilon_M(\vec{r} - \vec{r}')$ is well-established.^{37,43-45} It involves the inversion of the $\epsilon_{G,G'}(q)$ matrix to extract the macroscopic dielectric including local field effects $\epsilon(q) = 1/\epsilon_{0,0}^{-1}(q)$. On the other hand, the macroscopic dielectric constant computed without inversion does not contain local field effects. The same connection between the microscopic and macroscopic quantities is realized when the microscopic field is averaged over a cell volume in real space, thus keeping only Fourier components inside the Brillouin zone.⁴³⁻⁴⁵ Local fields effects are taken into account for the macroscopic dielectric constant computed in this work. However, it should be noticed that non-local effects on the self-energy cannot be evaluated from $\epsilon_M(q)$ in periodic solids, since these effects arise typically over a bond length.⁴²

The aim of the present work is to propose an approximate evaluation of self-energy corrections $\delta\Sigma$ in an heterostructure, by going beyond the abrupt dielectric interface model.^{15,35,36} Self-energy bulk contributions to the various properties of quasi-particles are supposed to be already described (electronic band gap, effective masses, etc.). Then, self-energy corrections are expected to be negligible far away from the interfaces. These corrections are related classically for abrupt interfaces, either to imaginary image charges placed in virtually homogeneous media, or to surface charge densities located at the interfaces. The abrupt dielectric interface model has one main advantage: it can be used to evaluate these contributions solely from dielectric properties of bulk materials and dielectric continuum theory,^{35,36} without any input from

ab initio modelling. However it can only be considered as a rough approximation and is well-known to lead to an unphysical divergence of the dielectric self-energy profile close to the interfaces. In order to understand the origin of this divergence and cure most of the models deficiencies without relying on a complete *ab initio* description, it is necessary to recall the basic ingredients of self-energy correction within the abrupt interface model. Within this description, self-energy corrections for a test charge e_0 are equivalent to a local potential acting on the charge. This is obtained by solving the Poisson equation for the electrostatic potentials in the heterostructure and in the bulk and taking the limit ($\vec{r} = \vec{r}_0$):^{35,36,47}

$$\delta\Sigma(\vec{r}_0) = \lim_{\vec{r} \rightarrow \vec{r}_0} \frac{1}{2} e_0 (V(\vec{r}, \vec{r}_0) - V_{bulk}(\vec{r}, \vec{r}_0)).$$

Where the classical screened potential equivalent to W in the GW approximation is:

$$W(\vec{r}, \vec{r}_0) = V(\vec{r}, \vec{r}_0) - V_{bulk}(\vec{r}, \vec{r}_0).$$

In a layered heterostructure, it is usual to define the planar average of the self-energy corrections $\delta\Sigma(z_0)$ which can be evaluated either from charge images in special cases³⁶ or, more generally, from the transverse Fourier transform of the electrostatic potential produced at position z by a charge e_0 located at position z_0 :³⁵

$$\delta\Sigma(z_0) = \frac{e_0}{4\pi} \int_0^\infty (V(q, z, z_0) - V_{bulk}(q, z, z_0))_{z \rightarrow z_0} q dq$$

$$V(r_t, z, z_0) = \frac{1}{2\pi} \int_0^\infty V(q, z, z_0) J_0(q, r_t) q dq$$

where $J_0(q, r_t)$ is a Bessel function and r_t is the in-plane distance between the two positions. The inhomogeneous Poisson equation yielding $V(q, z, z_0)$ is:

$$\frac{\partial}{\partial z} \left(\epsilon(z) \frac{\partial}{\partial z} (V(q, z, z_0)) \right) - q^2 \epsilon(z) V(q, z, z_0) = -e_0 \delta(z - z_0).$$

For a bulk homogeneous material, an analytical solution of this equation is

$$V_{bulk}(q, z, z_0) = \frac{e^{-q|z-z_0|}}{2q\epsilon}.$$

It shows that the knowledge of the dielectric constant profile $\epsilon(z)$ along a heterostructure is necessary to calculate $V(q, z, z_0)$ and the self-energy corrections. In the abrupt dielectric interface model, the dielectric profile is constructed piecewise from bulk dielectric constants.^{15,35}

A first inconsistency of the abrupt interface model is that all the information related to the interface nature are neglected, whereas self-energy corrections are expected to be maximum

on the interface and related to an interface induced charge density. The second fundamental inconsistency of this simplified representation of dielectric heterostructures, is the implicit incomplete Fourier filtering of the induced densities. Indeed, the underlying assumption leading to bulk constant values for the dielectric profile in bulk regions, corresponds to an effective nanoscale averaging or Fourier filtering with a critical wavevector related to the size of the Brillouin zone of the bulk materials. A step variation of the dielectric profile at interfaces is thus not consistent with this implicit assumption. Fully consistent nanoscopic dielectric profiles should be only properly defined with smooth variations across the interfaces. We propose in our model to take into account the nature of the interface and simultaneously cure the divergence problem of the self-energy correction by a proper nanoscale averaging of the induced density across all the heterostructure profile.

This prompts a general comment about non-locality and computation of self-energy corrections from dielectric continuum theory. The classical expression of self-energy corrections $\delta\Sigma(z_0)$ defined above, is local by construction, but the screened interaction $W(q, z, z_0)$ computed from the abrupt interface model^{35,36} is non-local due to the dielectric inhomogeneity of the heterostructure. Such expressions for $W(q, z, z_0)$ can thus be used to compute semi-classical non-local self-energy operator $\delta\Sigma(q, z, z_0)$ beyond the classical approach, and formally equivalent to the *ab initio* GW approximation.^{38,48} However, this procedure requires the precise knowledge of the single-particle wavefunctions and the one-electron Green functions. This has been done for empirical plane waves⁴⁸ and more recently for qualitative analysis of *ab initio* results.³⁸ However as indicated before, the non-local screened interaction $W(q, z, z_0)$, leads to unphysical effects close to the interface for step-like variation of the dielectric profile. It is expected to reproduce non-locality properties only far from the interface.³⁸ In this work, a more accurate representation of the dielectric profile is proposed but this procedure is not as complete as a full *ab initio* approach, since part of the information on non-locality is lost by the nanoscale averaging, especially for local field effects removed at the interface. The computation of self-energy corrections is performed in this work only for the local $\delta\Sigma(z_0)$ quantity, without detailed computations of the one-electron Green function. The dielectric constant profiles are piecewise discretized $\epsilon_i(z)$ and electric continuity relations are considered between the segments to calculate $V(q, z, z_0)$.

A DFT method based on polarization variation in response to a finite electric field was proposed recently to extract dielectric profiles in heterostructures.^{15,49} It avoids the complete determination of the dielectric matrix. The induced variation of the planar averaged electronic density is first computed by $\delta\rho_{ind}(z) = \rho(z)|_{E_{ext}^-} - \rho(z)|_0$. The induced polarization is then

given by the partial integration of

$$\frac{dp_{ind}(z)}{dz} = -\delta\rho(z).$$

In order to identify the localized contributions to the induced polarization, maximally localized Wannier functions were computed from the plane wave representation of the DFT solutions. As shown by one of the authors,¹⁵ this procedure also smoothes the atomic scale fluctuations of the charge density yielding essentially a nanoscale description of the dielectric property. It was nevertheless possible to study the influence of oxidation states of Si atoms located at the Si/SiO₂ interface.¹⁵ The method used in this work is similar, except for the representation of the DFT solutions directly in a localized basis functions.^{25–27} It is necessary to add a nanoscale averaging step to obtain a result equivalent to maximally localized Wannier functions. However, the initial DFT computation is computationally less demanding, especially for the representation of vacuum layers. The nanoscale average of the dielectric constant profile is necessary to make a proper connection with the macroscopic dielectric constant of the bulk material in the middle of the CNPL.

The dielectric nanoscale quantities are obtained in the present work by the simultaneous transverse and nanoscale averaging procedures.²⁵ The initial step of the DFT computational procedure is a study of the variation of the total induced dipole $m_z(L)$ of a 1D array of CNPL as a function of the array period. In each case, the total induced dipole of a CNPL is calculated by performing two DFT computations, with and without an external electric field.

The external electric field value is chosen to be equal to $E_{ext} = 0.025$ V/Å in the present work (we checked that the induced dipole have a linear variation as a function of E_{ext}). The slope of the inverse dipole variation as a function of $1/L$, is equal to $1/(\epsilon_0 \cdot E_{ext})$.²⁵ The induced dipole of an isolated CNPL m_z is obtained by extrapolating $1/L$ to 0. A graphical representation is to be found in the Electronic Supplementary Information (Figure ESI1). This procedure is simple and faster than specific implementations available in others codes.^{23,24} The key point is that it takes full advantage of the costless representation of vacuum sheets between CNPL in a strictly localized basis sets, as in SIESTA,²⁶ by comparison to plane waves.^{23,24} The $m_z(L)/m_z$ ratio is used to correct the induced polarisation profile from the interaction between CNPL (vide infra). Fig. 4 presents the variation of the induced dipole for isolated CNPL slabs as a function of CNPL thickness in the case of the 2×1 (001) surface reconstruction. It is then possible to deduce from a simple linear interpolation $m_z = n_{cell} a_{cell} P_{bulk} + m_{surf}$ both the bulk polarisation density P_{bulk} and the surface induced dipole m_{surf} . The bulk dielectric constant ϵ_∞ can then be evaluated from the bulk polarisation

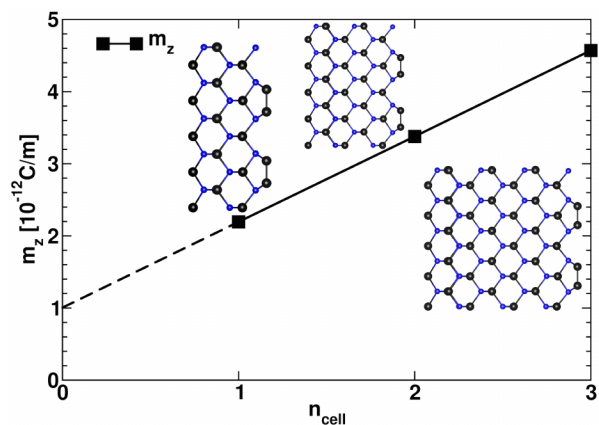


Fig. 4 Variation of the induced dipole m_z for isolated CNPL slabs with increasing thickness. The external electric field is $E_{ext} = 0.025$ V/Å. The repeated unit n_{cell} contains two CdSe ML. The slab is terminated on both sides by a 2×1 (001) surface reconstruction based on Cd dimers. The extrapolation for $n_{cell} = 0$ corresponds to the surface induced dipole m_{surf} .

density:

$$\epsilon_\infty = \frac{\epsilon_0 E_{ext}}{\epsilon_0 E_{ext} - P_{bulk}}.$$

We find that the calculated value for the bulk dielectric constant is $\epsilon_\infty = 6.7$ in fair agreement with the experimental value of 6.2.

In order to extract a dielectric constant profile along the CNPL stacking axis, the electronic density data obtained in the DFT computation are analyzed in four steps (Fig. 5).

- (i) The electronic density $\rho(z)$ is averaged in the plane perpendicular to the stacking axis (blue lines in Fig. 5). A nanoscale average along the stacking axis⁵⁰ is then carried out for the computation of the dielectric constant. The optimal filter function length with a square shape is determined from a study of the Hartree potential profile in the middle of the CNPL (Figure ESI2). It is equal to 0.32 nm (1 ML) in good agreement with the definition of macroscopic internal field in a solid (vide infra).
- (ii) The induced electronic density is calculated by subtracting the results of two DFT computations, with and without the external electric field $\delta\rho_{ind}(z) = \rho(z)|_{E_{ext}^-} - \rho(z)|_0$.
- (iii) The induced polarisation $p_{ind}(z)$ is calculated by the partial integration of the induced electronic density

$$\frac{dp_{ind}(z)}{dz} = -\delta\rho(z)$$

and correction from the interaction between CNPLs by the $m_z(L)/m_z$ factor. It can be numerically checked that

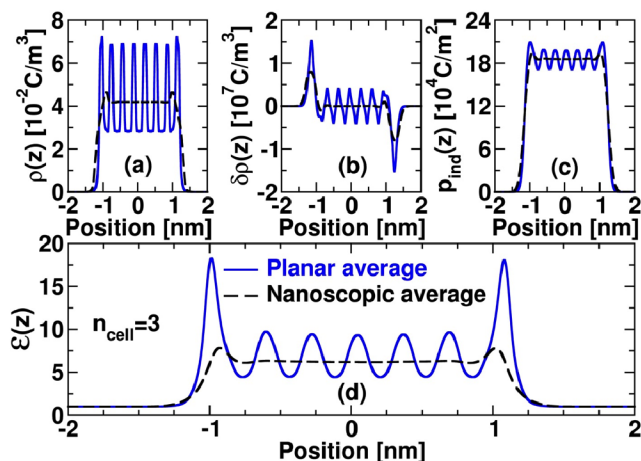


Fig. 5 Four-step procedure to extract a dielectric constant profile. (a) Variations of the charge density $\rho(z)$. (b) Induced charge density $\delta\rho(z)$. (c) Polarisation $p_{ind}(z)$ and (d) dielectric constant profile $\varepsilon(z)$ as a function of the position along the CNPL stacking axis (isolated slab, $n_{cell} = 3$). The external electric field is $E_{ext} = 0.025$ V/Å for curves (b-d). Blue lines correspond to planar averages quantities. An additional nanoscale average is used along the stacking axis for black dotted curves. The filter function length is equal to 0.32 nm (1 ML) (see text and Figure S2).

the total induced dipole for a CNPL (Fig. 4) is correctly given by

$$m_z = \int_{-\infty}^z p_{ind}(z) dz.$$

(iv) The nanoscopic average of the dielectric constant profile $\varepsilon(z)$ is calculated from

$$\varepsilon_{\infty}(z) = \frac{\varepsilon_0 E_{ext}}{\varepsilon_0 E_{ext} - p_{ind}(z)}.$$

The result computed from only a planar average of $p_{ind}(z)$ is also reported for comparison (blue line).

Fig. 6 presents the dielectric profiles calculated from the empirical abrupt model, and from the atomistic description of the three different coating of the thinnest CNPL ($n_{cell} = 1$). Fig. 6-a corresponds to the commonly used abrupt model with a permittivity set at the bulk value, *i.e.* 6.2, in the nanoplatelet. In contrast with that model, the atomic description of the reconstructed surface shows a peak at the edge of the CNPL with $\varepsilon(z)$ reaching 7.8, it is followed by a drop at 6.1 and a new maximum at the middle of the CNPL being 6.4. For the H-passivated surface one can also observe smaller peaks at the edge with a maximum value of 6.8. The drop causes a local minimum at the heart of the slab with a value of 6.1. The behavior is different with the AcO-passivated surface which exhibits a very smooth dielectric profile. From that compar-

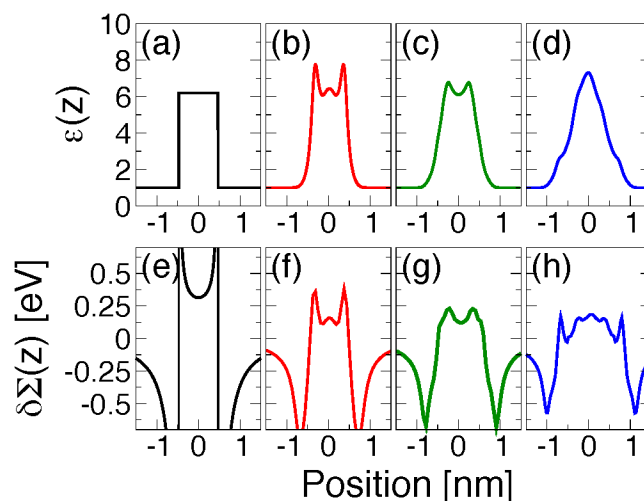


Fig. 6 (a-d) Variations of the nanoscale dielectric constant $\varepsilon(z)$ as a function of the position along the CNPL stacking axis (isolated slab, $n_{cell} = 1$) for (a) the abrupt model, (b) the reconstructed, (c) the H-passivated, and (d) the AcO-passivated surface. (e-h) Variations of the self-energy $\delta\Sigma(z)$ related to dielectric confinement for the corresponding surfaces.

ative study, one can deduce that the best surface passivation is obtained by molecular coating of the surface.

The reconstructed, H-passivated and AcO-passivated surfaces show very different polarisability. The distinction is to be related to the one in the density of states projected (PDOS) either on surface Cd atoms or AcO molecules with and without an electric field (Fig. 7). Indeed, with the reconstructed surface it is clear that the surface Cd dimers yield a strong modification of the electronic DOS very close to the valence band maximum (Fig. 7-a), whereas with the molecular coating (Fig. 7-c) the molecular electronic states response to the field is spread over a wide energy range.

In order to reach the planar average of the self-energy $\delta\Sigma(z_0)$ from our atomistic description, we use a special numerical procedure involving a transfer matrix approach starting from the exact solution for three-dielectric media with planar interfaces.^{35,47}

Figures 6 (e-h) display the results for the abrupt model and the three CNPLs ($n_{cell} = 1$). The model with abrupt interfaces¹⁵ leads to larger self-energy corrections at the center of the CNPL. Indeed, the value is found to be 0.31 eV for the model whereas it is only around half less for the systems with atomistic description. For the non-passivated and the H-passivated structures the behavior of $\delta\Sigma$ is similar to the one of ε . For the reconstructed (2×1) surface, $\delta\Sigma$ reaches a peak at the edge of the CNPL (0.36 eV) followed by a minimum at 0.11 eV and a local maximum is found at the middle of the CNPL with $\delta\Sigma = 0.16$ eV. For the H-passivated surface,

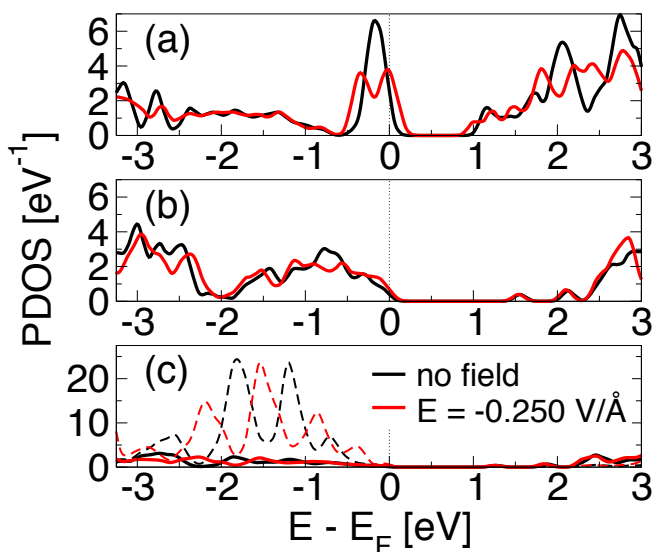


Fig. 7 Projected density of states (PDOS) for surface Cd atoms (solid lines) and AcO molecules (dashed lines) with ($E = -0.250$ V/Å, red lines) and without (black lines) electric field for $n_{cell} = 1$ with (a) the reconstructed, (b) the H-passivated, and (c) the AcO-passivated surfaces. The electric field has been exaggerated to enhance its effects on the PDOS.

we observe a shouldering around the position of the H atoms, then a maximum of 0.22 eV at the edge of the nanoplatelet and a minimum of 0.12 eV at the middle. The AcO-passivated CNPL presents a slightly distinct picture. Indeed we find a high self-energy correction at the position of the molecules with peaks reaching 0.17 eV. It is then followed by a small dip that goes to slightly negative values at the edge of the CdSe slab and $\delta\Sigma$ reaches a maximum at the center with a value of 0.19 eV. The fluctuations of the self-energy are small in the middle of the CNPL.

In the dielectric profile as well as in the self-energy profile, the abrupt model delivers good qualitative pictures. Still, it cannot provide with the subtlety imposed by the variety of surface coatings of CdSe CNPL.

Finally, we consider the influence of CNPL thickness in Fig. 8. The same dielectric constant value is found in the middle of the CNPL and the variation of the dielectric profiles close to the surface are also similar (Fig. 8-a). It is then not surprising that the increase of the self-energy in the middle of the CNPL when going from thicker to thinner CNPL is related to dielectric confinement effect. Such a result is qualitatively predicted from abrupt interface modeling of the CNPL. However, this model overestimates the effect of dielectric confinement on the renormalization of mono-electronic state energies and the electronic band gap. One may conversely also infer that additional dielectric contributions to excitonic binding en-

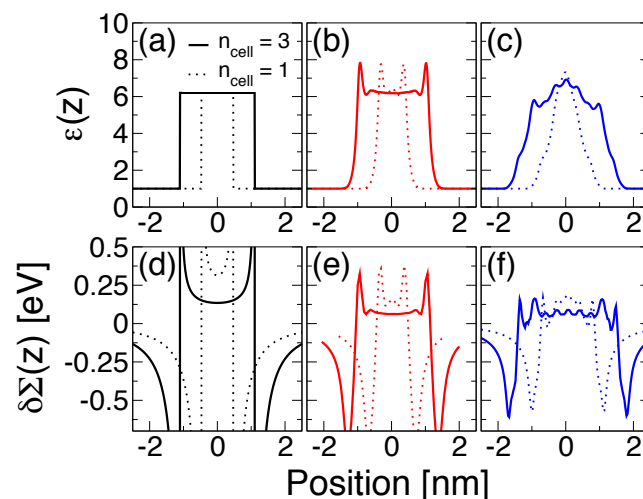


Fig. 8 (a-c) Variations of the nanoscale dielectric constant $\epsilon(z)$ as a function of the position along the CNPL stacking axis (isolated slab, $n_{cell} = 3$) for (a) the abrupt model, (b) the reconstructed, and (c) the AcO-passivated surface. The solid and dotted lines correspond to thin ($n_{cell} = 1$) and thicker ($n_{cell} = 3$) CNPL, respectively. (d-f) Same with the self-energy $\delta\Sigma(z)$.

ergy are probably smaller than the one predicted in previous studies from the abrupt interface model.^{14,15}

Conclusion

In summary, based on DFT calculations and continuum approaches, we proposed a description of CNPL electronic band structure including the influence of electronic surface states. Our study describes the basic concepts for the modeling of dielectric confinement beyond the standard abrupt interface model, including CNPL thickness and atomic structure of the surface. More generally, the method presented in this paper is also designed to bridge empirical and DFT methods applied to simulate hybrid nano-objects with 2D electronic properties. Dielectric properties of materials result of an interplay between quantum and size effect. The quantum confinement remains always the main effect. In most cases, the influence of the dielectric confinement will only show off for ultra-thin CNPL. AcO molecular coating in a tilted bridge configuration, has a beneficial effect on the electronic properties of CNPL, leading to an electronic band gap free of surface electronic states as well as an optimal surface coverage. These two effects are proposed to explain the reduced blinking in CdSe CNPL by comparison to CdSe CNC. This theoretical study opens the way toward more precise atomistic description of the CNPL and any hybrid system exhibiting 2D electronic properties, as well as dielectric confinement effect.

Acknowledgement

We wish to thank C. Katan and P. Voisin for stimulating and fruitful discussions.

References

- R. Dingle, W. Wiegmann and C. H. Henry, *Phys. Rev. Lett.*, 1974, **33**, 827.
- L. L. Chang, L. Esaki and R. Tsu, *Appl. Phys. Lett.*, 1974, **24**, 593.
- J. Faist, F. Capasso, D. L. Sivco, C. Sirtori, A. L. Hutchinson and A. Y. Cho, *Science*, 1994, **264**, 553.
- J. P. van der Ziel, R. Dingle, R. C. Miller, W. Wiegmann and W. A. Nordland Jr., *Appl. Phys. Lett.*, 1975, **26**, 463.
- R. D. Dupuis, P. D. Dapkus, N. Holonyak Jr., E. A. Rezek and R. Chin, *Appl. Phys. Lett.*, 1978, **32**, 295.
- B. F. Levine, K. K. Choi, C. G. Bethea, J. Walker and R. J. Malik, *Appl. Phys. Lett.*, 1987, **50**, 1092.
- M. Guézo, S. Loualiche, J. Even, A. Le Corre, H. Folliot, C. Labbé, O. Dehaese and G. Dousselin, *Appl. Phys. Lett.*, 2003, **82**, 1670.
- S. Ithurria, M. D. Tessier, R. P. S. M. Lobo, B. Dubertret and A. L. Efros, *Nature Mater.*, 2011, **10**, 936.
- M. D. Tessier, B. Mahler, B. Nadal, H. Heuclin, S. Pedetti and B. Dubertret, *Nano Lett.*, 2013, **13**, 3321.
- M. D. Tessier, P. Spinicelli, D. Dupont, G. Patriarche, S. Ithurria and B. Dubertret, *Nano Lett.*, 2014, **14**, 207.
- M. D. Tessier, C. Javaux, I. Maksimovic, V. Loriette and B. Dubertret, *ACS Nano*, 2012, **6**, 6751.
- C. Javaux, B. Mahler, B. Dubertret, A. Shabaev, A. V. Rodina, A. L. Efros, D. R. Yakovlev, F. Liu, M. Bayer, G. Camps, L. Biadala, S. Buil, X. Quelin and J.-P. Hermier, *Nature Nanotech.*, 2013, **8**, 206.
- L. T. Kunneman, M. D. Tessier, H. Heuclin, B. Dubertret, Y. V. Aulin, F. C. Grozema, J. M. Schins and L. D. A. Siebbeles, *J. Phys. Chem. Lett.*, 2013, **4**, 3574.
- A. W. Achtstein, A. Schliwa, A. Prudnikau, M. Hardzei, M. V. Artemyev, C. Thomsen and U. Woggon, *Nano Lett.*, 2012, **12**, 3151.
- R. Benchamekh, N. A. Gippius, J. Even, M. O. Nestoklon, J.-M. Jancu, S. Ithurria, B. Dubertret, A. L. Efros and P. Voisin, *Phys. Rev. B*, 2014, **89**, 035307.
- J. Zhou, J. Huang, B. G. Sumpter, P. R. C. Kent, H. Terrones and S. C. Smith, *J. Phys. Chem. C*, 2013, **117**, 25817.
- J. Even, L. Pedesseau, J.-M. Jancu and C. Katan, *J. Phys. Chem. Lett.*, 2013, **4**, 2999.
- J. Even, L. Pedesseau, J.-M. Jancu and C. Katan, *Phys. Status Solidi RRL*, 2014, **8**, 31.
- J. Even, L. Pedesseau, M.-A. Dupertuis, J.-M. Jancu and C. Katan, *Phys. Rev. B*, 2012, **86**, 205301.
- B. Meyer and D. Vanderbilt, *Phys. Rev. B*, 2001, **63**, 205426.
- F. Giustino and A. Pasquarello, *Phys. Rev. B*, 2005, **71**, 144104.
- B. Lee, C.-K. Lee, S. Han, J. Lee and C. S. Hwang, *J. Appl. Phys.*, 2008, **103**, 024106.
- G. Kresse and J. Furthmüller, *Phys. Rev. B*, 1996, **54**, 11169.
- P. Giannozzi, S. Baroni, N. Bonini, M. Calandra, R. Car, C. Cavazzoni, D. Ceresoli, G. L. Chiarotti, M. Cococcioni, I. Dabo, A. Dal Corso, S. de Gironcoli, S. Fabris, G. Fratesi, R. Gebauer, U. Gerstmann, C. Gougoussis, A. Kokalj, M. Lazzeri, L. Martin-Samos, N. Marzari, F. Mauri, R. Mazzarello, S. Paolini, A. Pasquarello, L. Paulatto, C. Sbraccia, S. Scandolo, G. Sclauzero, A. P. Seitsonen, A. Smogunov, P. Umari and R. M. Wentzcovitch, *J. Phys.: Condens. Matter*, 2009, **21**, 395502.
- N. Shi and R. Ramprasad, *Phys. Rev. B*, 2006, **74**, 045318.
- J. M. Soler, E. Artacho, J. D. Gale, A. García, J. Junquera, P. Ordejón and D. Sánchez-Portal, *J. Phys.: Condens. Matter*, 2002, **14**, 2745.
- E. Artacho, E. Anglada, O. Diéguez, J. D. Gale, A. García, J. Junquera, R. M. Martin, P. Ordejón, J. M. Pruneda, D. Sánchez-Portal and J. M. Soler, *J. Phys.: Condens. Matter*, 2008, **20**, 064208.
- J. P. Perdew, K. Burke and M. Ernzerhof, *Phys. Rev. Lett.*, 1996, **77**, 3865.
- N. Troullier and J. L. Martins, *Phys. Rev. B*, 1991, **43**, 1993.
- E. Artacho, D. Sánchez-Portal, P. Ordejón, A. García and J. M. Soler, *phys. stat. sol. (b)*, 1999, **215**, 809.
- J. A. Appelbaum and D. R. Hamann, *Surf. Sci.*, 1978, **74**, 21.
- N. Sanada, S. Mochizuki, S. Ichikawa, N. Utsumi, M. Shimomura, G. Kaneda, A. Takeuchi, Y. Suzuki, Y. Fukuda, S. Tanaka and M. Kamata, *Surf. Sci.*, 1999, **419**, 120.
- O. Voznyy, *J. Phys. Chem. C*, 2011, **115**, 15927.
- O. Voznyy, S. M. Thon, A. H. Ip and E. H. Sargent, *J. Phys. Chem. Lett.*, 2013, **4**, 987.
- R. G. Barrera, O. Guzmán and B. Balaguer, *Am. J. Phys.*, 1978, **46**, 1172.
- M. Kumagai and T. Takagahara, *Phys. Rev. B*, 1989, **40**, 12359.
- G. Strinati, *Rivista del Nuovo Cimento*, 1988, **11**, 1.
- C. Freysoldt, P. Eggert, P. Rinke, A. Schindlmayr and M. Scheffler, *Phys. Rev. B*, 2008, **77**, 235428.
- J. Lischner, D. Vigil-Fowler and S. G. Louie, *Phys. Rev. Lett.*, 2013, **110**, 146801.
- P. García-González and R. W. Godby, *Comput. Phys. Commun.*, 2001, **137**, 108.
- M. S. Hybertsen and S. G. Louie, *Phys. Rev. B*, 1986, **34**, 5390.
- R. W. Godby, M. Schlüter and L. J. Sham, *Phys. Rev. B*, 1988, **37**, 10159.
- S. L. Adler, *Phys. Rev.*, 1962, **126**, 413.
- N. Wiser, *Phys. Rev.*, 1963, **129**, 62.
- R. Del Sole and E. Fiorino, *Phys. Rev. B*, 1984, **29**, 4631.
- R. Resta and K. Kunc, *Phys. Rev. B*, 1986, **34**, 7146.
- F. Stern, *Phys. Rev. B*, 1978, **17**, 5009.
- R. G. Barrera and C. B. Duke, *Phys. Rev. B*, 1976, **13**, 4477.
- F. Giustino, P. Umari and A. Pasquarello, *Phys. Rev. Lett.*, 2003, **91**, 267601.
- J. Junquera, M. H. Cohen and K. M. Rabe, *J. Phys.: Condens. Matter*, 2007, **19**, 213203.